



A Model for Jet-Surface Interaction Noise Using Physically Realizable Upstream Turbulence Conditions

*Mohammed Z. Afsar
Imperial College London, London, United Kingdom*

*Stewart J. Leib
Ohio Aerospace Institute, Cleveland, Ohio*

*Richard F. Bozak
Glenn Research Center, Cleveland, Ohio*

NASA STI Program . . . in Profile

Since its founding, NASA has been dedicated to the advancement of aeronautics and space science. The NASA Scientific and Technical Information (STI) Program plays a key part in helping NASA maintain this important role.

The NASA STI Program operates under the auspices of the Agency Chief Information Officer. It collects, organizes, provides for archiving, and disseminates NASA's STI. The NASA STI Program provides access to the NASA Technical Report Server—Registered (NTRS Reg) and NASA Technical Report Server—Public (NTRS) thus providing one of the largest collections of aeronautical and space science STI in the world. Results are published in both non-NASA channels and by NASA in the NASA STI Report Series, which includes the following report types:

- TECHNICAL PUBLICATION. Reports of completed research or a major significant phase of research that present the results of NASA programs and include extensive data or theoretical analysis. Includes compilations of significant scientific and technical data and information deemed to be of continuing reference value. NASA counter-part of peer-reviewed formal professional papers, but has less stringent limitations on manuscript length and extent of graphic presentations.
- TECHNICAL MEMORANDUM. Scientific and technical findings that are preliminary or of specialized interest, e.g., “quick-release” reports, working papers, and bibliographies that contain minimal annotation. Does not contain extensive analysis.
- CONTRACTOR REPORT. Scientific and technical findings by NASA-sponsored contractors and grantees.
- CONFERENCE PUBLICATION. Collected papers from scientific and technical conferences, symposia, seminars, or other meetings sponsored or co-sponsored by NASA.
- SPECIAL PUBLICATION. Scientific, technical, or historical information from NASA programs, projects, and missions, often concerned with subjects having substantial public interest.
- TECHNICAL TRANSLATION. English-language translations of foreign scientific and technical material pertinent to NASA's mission.

For more information about the NASA STI program, see the following:

- Access the NASA STI program home page at <http://www.sti.nasa.gov>
- E-mail your question to help@sti.nasa.gov
- Fax your question to the NASA STI Information Desk at 757-864-6500
- Telephone the NASA STI Information Desk at 757-864-9658
- Write to:
NASA STI Program
Mail Stop 148
NASA Langley Research Center
Hampton, VA 23681-2199



A Model for Jet-Surface Interaction Noise Using Physically Realizable Upstream Turbulence Conditions

*Mohammed Z. Afsar
Imperial College London, London, United Kingdom*

*Stewart J. Leib
Ohio Aerospace Institute, Cleveland, Ohio*

*Richard F. Bozak
Glenn Research Center, Cleveland, Ohio*

Prepared for
Aviation 2015
sponsored by the American Institute of Aeronautics and Astronautics
Dallas, Texas, June 22–26, 2015

National Aeronautics and
Space Administration

Glenn Research Center
Cleveland, Ohio 44135

Acknowledgments

Mohammed Z. Afsar would like to thank financial support from Chapman Fellowship (2013-2014) at Imperial College London, Department of Mathematics and would like to thank useful discussions with Professor W. Devenport at Virginia Tech. The work was also supported by the NASA Fundamental Aeronautics Program, High Speed Project.

Trade names and trademarks are used in this report for identification only. Their usage does not constitute an official endorsement, either expressed or implied, by the National Aeronautics and Space Administration.

This work was sponsored by the Fundamental Aeronautics Program at the NASA Glenn Research Center.

Level of Review: This material has been technically reviewed by technical management.

Available from

NASA STI Program
Mail Stop 148
NASA Langley Research Center
Hampton, VA 23681-2199

National Technical Information Service
5285 Port Royal Road
Springfield, VA 22161
703-605-6000

This report is available in electronic form at <http://www.sti.nasa.gov/> and <http://ntrs.nasa.gov/>

A Model for Jet-Surface Interaction Noise Using Physically Realizable Upstream Turbulence Conditions

Mohammed Z. Afsar
Imperial College London
London, SW7, United Kingdom

Stewart J. Leib
Ohio Aerospace Institute
Brook Park, Ohio 44142

Richard F. Bozak
National Aeronautics and Space Administration
Glenn Research Center
Cleveland, Ohio 44135

Abstract

This paper is a continuation of previous work in which a generalized Rapid Distortion Theory (RDT) formulation was used to model low-frequency trailing-edge noise. The research was motivated by proposed next-generation aircraft configurations where the exhaust system is tightly integrated with the airframe. Data from recent experiments at NASA on the interaction between high-Reynolds-number subsonic jet flows and an external flat plate showed that the power spectral density (PSD) of the far-field pressure underwent considerable amplification at low frequencies. For example, at the 90° observation angle, the low-frequency noise could be as much as 10 dB greater than the jet noise itself. In this paper, we present predictions of the noise generated by the interaction of a rectangular jet with the trailing edge of a semi-infinite flat plate. The calculations are based on a formula for the acoustic spectrum of this noise source derived from an exact formal solution of the linearized Euler equations involving (in this case) one arbitrary convected scalar quantity and a Rayleigh equation Green's function. A low-frequency asymptotic approximation for the Green's function based on a two-dimensional mean flow is used in the calculations along with a physically realizable upstream turbulence spectrum, which includes a finite decorrelation region. Numerical predictions of the sound field, based on three-dimensional RANS solutions to determine the mean flow, turbulent kinetic energy and turbulence length and time scales, for a range of subsonic acoustic Mach number jets and nozzle aspect ratios are compared with experimental data. Comparisons of the RANS results with flow data are also presented for selected cases. We find that a finite decorrelation region in the turbulence spectrum increases the low-frequency algebraic decay (the low frequency "roll-off") of the acoustic spectrum with angular frequency thereby producing much closer agreement with noise data for Strouhal numbers less than 0.1. Secondly, the large-aspect-ratio theory is able to predict the low-frequency amplification due to the jet-edge interaction reasonably well, even for moderate aspect ratio nozzles. We show also that the noise predictions for smaller aspect ratio jets can be fine-tuned using the appropriate RANS-based mean flow and turbulence properties.

Nomenclature

c sound speed
 c_∞ ambient sound speed
 D_J nozzle diameter

g	Green's function
I_ω	acoustic spectrum
k	turbulent kinetic energy
k_1	streamwise wavenumber
l_i	characteristic length scale
M	acoustic Mach number
Ma	jet acoustic Mach number
p	pressure
t	time
T	averaging time
U_c	convection velocity
V	source volume
v_i	velocity vector
\mathbf{x}	observer location
\mathbf{y}	source location
α	turbulence intensity
β	angle function
γ	specific heat ratio
δ_{ij}	Kronecker delta
ε	turbulence dissipation rate
$\boldsymbol{\eta}$	separation vector
ρ	density
θ	polar angle measured from jet axis
τ	time delay
ω	radian frequency
∇	gradient operator
$ $	absolute value

Subscripts

i,j,k,l	tensor indices = 1,2,3
\perp	transverse component

Superscripts

a	adjoint
$\bar{\quad}$	time average
\prime	fluctuating quantity
\sim	Favre average
$*$	complex conjugate

1.0 Introduction

Jet flows of technological interest are almost always close enough to, or sufficiently confined by, solid boundaries, so that the surface defining the boundary plays a direct role in the generation of sound, as well as its propagation. Understanding the basic physics behind this process is of considerable importance for present-day and future aircraft that may have complex engine installation geometries. The aim of this paper is to further develop a prediction method for the noise generated by the interaction of a

turbulent jet with the trailing edge of a flat plate. This problem serves as a model of one important aspect of engine-installation effects, namely the interaction of the exhaust jet with a wing. The prediction method is based on a self-consistent application of the nonhomogeneous Rapid-distortion theory (RDT) introduced recently in Reference 1 (hereafter referred to as GAL).

Experiments conducted by Olsen and Boldman (Ref. 2) and Wang (Ref. 3) showed that the presence of an external surface enhanced the noise produced by the jet alone for observation points on the same side as the jet flow. In Reference 2 it was shown that including mean flow interaction effects significantly improves the accuracy of noise predictions for a jet near an external surface compared with approaches that neglect this effect (Ref. 4). Recent experiments at the NASA Glenn Research Center (Refs. 5, 6, 7, 8, and 9) have modelled the jet-wing interaction problem as a jet flow interacting with a trailing edge of an external plate. The power spectral density of the far-field pressure (PSD) was measured for unheated, high Reynolds number, jet flows across a range of acoustic Mach numbers when the trailing edge was positioned above/beneath the flow at various axial/radial locations relative to the nozzle center line.

The findings of Reference 6 have generally confirmed the trends of References 2 and 3. In particular, at low frequencies, the PSD is considerably amplified compared to the free jet, and this effect is greatest at large polar observation angles to the jet axis (i.e., near 90°); see figures 6 and 8 in Reference 6. This low-frequency amplification effect has been called “jet-surface interaction” noise by Brown (Ref. 10), owing to its observed dipole characteristic and structural difference to high-frequency noise shielding and reflection. In Reference 10, Brown developed an empirical model for jet-surface interaction noise and extracted the noise due to the jet/trailing edge interaction from measurements of the total noise in various jet-plate configurations using the expected dipole characteristics of the edge noise source.

In this paper we use the general theory developed in Reference 1 to model the jet-surface interactions using RDT. Rapid Distortion Theory uses linear analysis to study the interaction of turbulence with, for example, solid surfaces. It applies whenever the turbulence intensity is small and the time scale for the interaction is short compared to the turn-over time of the turbulent eddies, i.e., the time over which nonlinear interactions and viscous dissipation take place. The problem is then linear and inviscid and is governed by the compressible Rayleigh equation.

An initial application of the general theory to the jet-surface interaction problem was included in GAL. Here, we further develop the prediction method by introducing a more realistic model for the statistics of the upstream turbulence whose interaction with the plate edge generates noise. The modelling approach is similar to that in Reference 13, but used here for the (second-order) transverse velocity auto covariance. In particular, we show that a region of negative correlation (or ‘decorrelation’) in this quantity directly impacts the low-frequency algebraic decay (often referred to as the ‘roll-off’) of the edge-generated noise and provides better agreement with experimental data than our previous results. The presence of such negative regions in second-order correlation has been known for some time (Ref. 14). This result has implications for trailing-edge noise control.

The prediction capabilities of the method are further developed by using results from Reynolds-averaged Navier-Stokes (RANS) solutions to obtain the mean flow and inform the source model, in particular to obtain the turbulent length scales and source amplitude. The use of RANS solutions also allows these flow quantities to vary with flow conditions and geometry. The RANS solutions are obtained using the SolidWorks Flow Simulation software (Dassault Systèmes SolidWorks Corporation) (Refs. 11 and 12), which provides relatively fast solutions for the geometries of interest. As a check on the quality of these results, we include comparisons with measured flow data (Ref. 7) for selected cases.

In the next section we summarize the main features of nonhomogeneous RDT introduced in GAL and describe how this theory can be used for the trailing-edge noise problem. As mentioned above, there are two novel features of the present paper as compared to the trailing edge model in GAL. Firstly, we use a

more advanced turbulence model for the two-point correlation of the transverse velocity fluctuations. Secondly, noise predictions using results from RANS solutions to obtain the mean flow profile and turbulent kinetic energy near the trailing edge are presented and compared with experimental data taken at NASA Glenn.

In Section 2.0, we briefly review the relevant parts of the GAL analysis used in this work. In Section 3.0, we introduce the new model for the transverse velocity correlations and present the corresponding formula for the acoustic spectrum. In Section 4.0, we illustrate some generic features of the model using an analytically prescribed mean flow. The impact of the new source model on the low-frequency “roll-off” of the spectrum and comparisons with the model of GAL are shown. In Section 5.0, the use of SolidWorks software to obtain RANS solutions for a rectangular jet near the edge of flat plate is described. Results from these solutions are compared with experimental data taken at NASA Glenn (Ref. 7) for the mean flow and turbulent kinetic energy distributions near the edge of the plate. In Section 6.0, we present comparisons of noise predictions using the model developed in this paper, with the SolidWorks RANS solutions as input, with data taken at NASA Glenn. Conclusions and discussion of potential future work is given in Section 7.0.

2.0 Review of the GAL Formulation

2.1 Euler Equations for Small-Amplitude Motion

Let all lengths and velocities be nondimensionalized by D_J and U_J , respectively; time by D_J/U_J and pressure by $\rho_J U_J^2$, where ρ_J and U_J are flow density and velocity, respectively, at nozzle exit and D_J is an appropriate reference length scale (such as the nozzle exit equivalent diameter). The flow Reynolds number is assumed to be large, i.e., $R = U_J D_J / \nu \gg O(1)$ and the turbulence Reynolds number is fixed at order 1, i.e., $R_T = \alpha R = O(1)$; where ν is the kinematic viscosity and $\alpha \equiv |\mathbf{v}'|/U_J \ll O(1)$ is the turbulence intensity of the upstream flow. $|\mathbf{v}'|$ is the magnitude of the local rms turbulence velocity.

We suppose that the flow is inviscid and nonheat conducting and assume an ideal gas so that the entropy is proportional to $\ln(p/\rho^\gamma)$ and the squared sound speed is $\gamma p/\rho$, where p denotes the pressure, ρ the density and γ the specific heat ratio. The inviscid pressure $p' = p - p_0$ and momentum flux perturbations, $u_i \equiv \rho v'_i$, where v'_i denotes the velocity perturbation, on a transversely sheared mean flow with pressure $p_0 = \text{constant}$, velocity $U(\mathbf{y}_T)$ and mean sound speed squared c^2 , are governed by the linearized momentum and energy equations

$$\frac{D_0 u_i}{D\tau} + \delta_{ij} u_j \frac{\partial U}{\partial y_j} + \frac{\partial p'}{\partial y_i} = 0 \quad (1)$$

and

$$\frac{D_0 p'}{D\tau} + \frac{\partial c^2 u_j}{\partial y_j} = 0, \quad (2)$$

where, $\mathbf{y} = \{y_1, y_2, y_3\} = \{y_1, \mathbf{y}_T\}$, $\mathbf{y}_T = \{y_2, y_3\}$ and $D_0/D\tau \equiv \partial/\partial\tau + U \partial/\partial y_1$ denotes the convective derivative.

2.1.1 Integration of the Euler Equations (1) and (2)

Goldstein (Ref. 15) showed that Equation (1) will be satisfied for any function $\phi(\mathbf{y}, \tau)$ and any purely convected quantity, $\mathfrak{S}(\tau - y_1/U(\mathbf{y}_T), \mathbf{y}_T)$, when p' and u_i are determined by

$$p'(\mathbf{y}, \tau) = -\frac{D_0^3 \phi}{D\tau^3}(\mathbf{y}, \tau), \quad (3)$$

and

$$u_i(\mathbf{y}, \tau) = \left(\delta_{ij} \frac{D_0}{D\tau} - \delta_{i1} \frac{\partial U}{\partial y_j} \right) \lambda_j(\mathbf{y}, \tau) + \varepsilon_{ijk} \frac{1}{c^2} \frac{\partial U}{\partial y_j} \frac{\partial}{\partial y_k} \mathfrak{S} \left(\tau - \frac{y_1}{U(\mathbf{y}_T)}, \mathbf{y}_T \right), \quad (4)$$

where δ_{ij} denotes the Kronecker delta, ε_{ijk} the alternating tensor and

$$\lambda_j \equiv \frac{\partial}{\partial y_j} \frac{D_0 \phi}{D\tau} + 2 \frac{\partial U}{\partial y_j} \frac{\partial \phi}{\partial y_1} \quad (5)$$

is a kind of generalized particle displacement (Ref. 15, Eqs. 2.9 and 2.10).

The energy equation, (2), is then satisfied when the scalar $\phi(\mathbf{y}, \tau)$ is determined by:

$$\frac{D_0}{D\tau} \left[\frac{\partial}{\partial y_i} c^2 \left(\frac{\partial}{\partial y_i} \frac{D_0 \phi}{D\tau} + 2 \frac{\partial U}{\partial y_i} \frac{\partial \phi}{\partial y_1} \right) - \frac{D_0^3 \phi}{D\tau^3} \right] = 0, \quad (6)$$

which can be integrated to obtain,

$$L_a \phi = -\tilde{\omega}_c(\tau - y_1/U(\mathbf{y}_T), \mathbf{y}_T), \quad (7)$$

where

$$L_a \equiv \frac{D_0^3}{D\tau^3} - \frac{\partial}{\partial y_i} c^2 \left(\frac{\partial}{\partial y_i} \frac{D_0}{D\tau} + 2 \frac{\partial U}{\partial y_i} \frac{\partial}{\partial y_1} \right). \quad (8)$$

and $\tilde{\omega}_c(\tau - y_1/U(\mathbf{y}_T), \mathbf{y}_T)$ is another arbitrary, purely convected, quantity. GAL point out that the operator L_a is the adjoint to the Rayleigh operator,

$$L \equiv \frac{D_0}{D\tau} \left(\frac{\partial}{\partial y_i} c^2 \frac{\partial}{\partial y_i} - \frac{D_0^2}{D\tau^2} \right) - 2 \frac{\partial U}{\partial y_j} \frac{\partial}{\partial y_1} c^2 \frac{\partial}{\partial y_j}, \quad (9)$$

which is obtained by eliminating the momentum flux perturbation between (1) and (2) to derive a single equation for the fluctuating pressure

$$L p' = 0. \quad (10)$$

The solution to $\phi(\mathbf{y}, \tau)$ can then be found by solving (7) as a boundary value problem in terms of the Rayleigh equation Green's function (as shown in GAL)

$$L g(\mathbf{y}, \tau | \mathbf{x}, t) = \delta(\mathbf{y} - \mathbf{x}) \delta(\tau - t), \quad (11)$$

subject to appropriate boundary conditions, and the result inserted into (4) to obtain $u_i(\mathbf{y}, \tau)$.

2.2 Integral Solutions to the Euler Equations for Arbitrary Transversely Sheared Mean Flows

GAL showed that the formal complete solution to the nonhomogeneous Rapid Distortion Theory problem for the pressure perturbation, p' , is given by

$$p'(\mathbf{x}, t) = \int_{-T}^T \int_V \frac{D_0^3 g(\mathbf{y}, \tau | \mathbf{x}, t)}{Dt^3} \tilde{\omega}_c(\tau - y_1/U(\mathbf{y}_T), \mathbf{y}_T) d\mathbf{y} d\tau \quad (12)$$

(where T denotes a very large but finite time interval) when the solid surfaces S (which can be finite, semi-infinite or infinite in the streamwise direction) coincide with any level surfaces of the mean velocity profile (as in the trailing edge problem considered herein). The solution for p' in these cases is independent of the convected quantity $\mathfrak{G}(\tau - y_1)/U(\mathbf{y}_T), \mathbf{y}_T$.

The corresponding solution for the transverse momentum fluctuation is also independent of \mathfrak{G} and is given by

$$\rho v'_i(\mathbf{x}, t) \equiv u_i(\mathbf{x}, t) \frac{\partial U}{\partial x_i} / |\nabla U| = - \frac{\partial U / \partial x_i}{|\nabla U|} \int_{-T}^T \int_V g_i(\mathbf{y}, \tau | \mathbf{x}, t) \tilde{\omega}_c(\tau - y_1/U(\mathbf{y}_T), \mathbf{y}_T) d\mathbf{y} d\tau \quad (13)$$

where

$$g_i(\mathbf{y}, \tau | \mathbf{x}, t) \equiv \frac{D_0}{Dt} \left(\frac{\partial}{\partial x_i} \frac{D_0}{Dt} + 2 \frac{\partial U}{\partial x_i} \frac{\partial}{\partial x_1} \right) g(\mathbf{y}, \tau | \mathbf{x}, t). \quad (14)$$

This solution involves only the purely convected quantity $\tilde{\omega}_c(\tau - y_1/U(\mathbf{y}_T), \mathbf{y}_T)$, that can be specified as an input condition within a general boundary value problem involving inhomogeneous boundary conditions. The Green's function $g(\mathbf{y}, \tau | \mathbf{x}, t)$ is found by solving (11) with incoming wave behavior as $|\mathbf{y}| \rightarrow \infty$ and appropriate boundary conditions (on the bounding surfaces S that generate volume V) for (12) and (13) to hold.

2.3 Green's Function Splitting

Following GAL, we can think of solution (12) as being the sum of an input disturbance and downstream response (Figure 1). The trailing-edge noise (or the output response) is generated by an input interacting with streamwise changes in boundary conditions at the plate edge. GAL divided the Rayleigh equation Green's function that appears in (12) into the components,

$$g(\mathbf{y}, \tau | \mathbf{x}, t) = g^{(0)}(\mathbf{y}, \tau | \mathbf{x}, t) + g^{(s)}(\mathbf{y}, \tau | \mathbf{x}, t) \quad (15)$$

where $g^{(0)}(\mathbf{y}, \tau | \mathbf{x}, t)$ is now defined on all space and satisfies

$$\hat{n}_i \partial \left[D_0^3 g^{(0)}(\mathbf{y}, \tau | \mathbf{x}, t) / Dt^3 \right] / \partial y_i = 0 \quad \text{for } \mathbf{y}_T \in S \quad (16)$$

where S is a doubly infinite surface and $\hat{\mathbf{n}}(\mathbf{y}) = \{\hat{n}_i\}(\mathbf{y})$ is the unit outward-drawn normal to S .

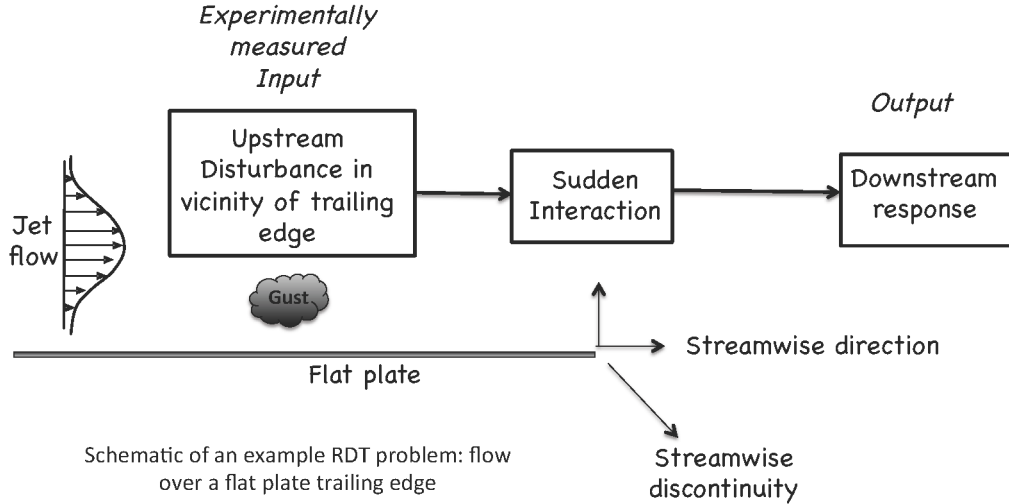


Figure 1.—Mathematical model of the jet-surface interaction noise.

Then, by (13), the corresponding transverse momentum flux is

$$\rho v_{\perp}^{\prime(0)}(\mathbf{x}, t) = -\frac{\partial U / \partial x_i}{|\nabla U|} \int_{-T}^T \int_V g_i^{(0)}(\mathbf{y}, \tau | \mathbf{x}, t) \tilde{\omega}_c \left(\tau - \frac{y_1}{U(\mathbf{y}_T)}, \mathbf{y}_T \right) dy d\tau \quad (17)$$

and then represents the input disturbance for the trailing-edge scattering problem and is referred to as the *gust solution*, i.e., a bounded hydrodynamic disturbance on a flow with streamwise homogeneous boundary conditions in the absence of any scattering surfaces. Although $\tilde{\omega}_c(\tau - y_1/U(\mathbf{y}_T), \mathbf{y}_T)$ is not a physically measurable quantity, Equation (17) provides an (in general) integral relation between $\tilde{\omega}_c(\tau - y_1/U(\mathbf{y}_T), \mathbf{y}_T)$ and the physical variable, $\rho v_{\perp}^{\prime(0)}(\mathbf{x}, t)$ that can, in principle, be inverted (using identity (1.97) in Goldstein (Ref. 16) to solve) for the Fourier transform of $\tilde{\omega}_c(\tau - y_1/U(\mathbf{y}_T), \mathbf{y}_T)$ in terms of the Fourier transform of $\rho v_{\perp}^{\prime(0)}(\mathbf{x}, t)$.

2.4 Relation Between the $\tilde{\omega}_c$ Spectrum and Measurable Turbulence Statistics

The correspondence our input gust (17) has to the actual upstream turbulence in a “real” trailing-edge noise problem can be reconciled as follows. We are assuming the relation between $\tilde{\omega}_c(\tau - y_1/U(\mathbf{y}_T), \mathbf{y}_T)$ and $\rho v_{\perp}^{\prime(0)}(\mathbf{x}, t)$ in the actual flow is the same as it would in an idealized mathematical representation of a transversely sheared mean flow where $R_T = \alpha R = O(1)$ everywhere in the flow and in which bounding surfaces present are doubly infinite in the streamwise direction (i.e., where the transverse boundary conditions are completely uniform in y_1). Hence the upstream boundary condition is determined on this streamwise homogeneous flow is assumed to be the same as that in the vicinity of trailing-edge where the “real” distortion actually takes place.

GAL showed that the inversion of (17) can be obtained analytically for a two-dimensional mean flow by computing the (temporal, streamwise and spanwise) Fourier transform of $\rho v_{\perp}^{\prime(0)}(\mathbf{x}, t)$ and relating it exactly to the Fourier transform of $\tilde{\omega}_c(\tau - y_1/U(\mathbf{y}_T), \mathbf{y}_T)$, but that this relation can only be specified at N

discrete transverse space points, say $x_2^{(1)}, x_2^{(2)}, \dots, x_2^{(N)}$, where $x_2^{(n)}$ is given by solutions to discrete equation, $U(x_2^{(n)}) = U(x_2)$, for $n = 1, 2, \dots, N$, leading to a matrix problem to determine the auto-covariance of the transform of $\tilde{\omega}_c(\tau - y_1/U(\mathbf{y}_T), \mathbf{y}_T)$ in terms of the auto-covariance of the transform of $\rho v_{\perp}^{(0)}(\mathbf{x}, t)$. For jet flows, such as those considered in the present paper, there are two such points and, following GAL, we take $(x_2^{(1)}, x_2^{(2)}) = y_d$, where y_d is the location where the velocity profile is maximum. In some sense, this gives an upper bound for the upstream boundary condition and allows the role of the decorrelation region to be assessed easily.

GAL used a uniformly valid low-frequency asymptotic solution for the gust Green's function in the relation between the Fourier transforms of $\rho v_{\perp}^{(0)}(\mathbf{x}, t)$ and $\tilde{\omega}_c(\tau - y_1/U(\mathbf{y}_T), \mathbf{y}_T)$ to obtain a relatively simple working formula relating the spectrum of the convected quantity $\tilde{\omega}_c(\tau - y_1/U(\mathbf{y}_T), \mathbf{y}_T)$,

$$S(y_2, \tilde{y}_2; k_3^{(s)}, \omega),$$

$$S(y_2, \tilde{y}_2; k_3, \omega) \equiv \frac{1}{2\pi} \int_{-\infty}^{\infty} \int_{-\infty}^{\infty} e^{i(\omega\tau - k_3\eta_3)} \langle \tilde{\omega}_c(t, y_2, y_3) \tilde{\omega}_c(t + \tau, \tilde{y}_2, y_3 + \eta_3) \rangle d\tau d\eta_3, \quad (18)$$

to the experimentally measurable transverse velocity spectrum

$$F_{\perp}(x_2, \tilde{x}_2 | y_2, \tilde{y}_2, \omega, k_3) = \frac{1}{(2\pi)^2} \int_{-\infty}^{\infty} \int_{-\infty}^{\infty} e^{-i(\omega\tau - k_3\eta_3)} f_{\perp}(x_2, \tilde{x}_2 | \omega/U(y_2), \omega/U(\tilde{y}_2), \eta_3, \tau) d\eta_3 d\tau \quad (19)$$

where

$$f_{\perp}(x_2, \tilde{x}_2 | k_1, \tilde{k}_1, \eta_3, \tau) \equiv \frac{1}{(2\pi)^2} \int_{-\infty}^{\infty} \int_{-\infty}^{\infty} e^{-i(x_1 k_1 - \tilde{x}_1 \tilde{k}_1)} \langle \rho v_{\perp}^{(0)}(\mathbf{x}, t) \rho v_{\perp}^{(0)}(\tilde{\mathbf{x}}_1, \tilde{x}_2, x_3 + \eta_3, t + \tau) \rangle dx_1 d\tilde{x}_1, \quad (20)$$

as,

$$S(y_2, \tilde{y}_2; k_3, \omega) = \frac{|U'(y_2)U'(\tilde{y}_2)| \left(1 + \frac{y_2 - y_d}{y_d} b_0\right) \left(1 + \frac{\tilde{y}_2 - y_d}{y_d} b_0\right) F_{\perp}(y_d, y_d | y_2, \tilde{y}_2, \omega, k_3)}{[U(y_2)U(\tilde{y}_2)] E(y_2; k_3, \omega) [E(\tilde{y}_2; k_3, \omega)]^*} \quad (21)$$

where

$$E(y_2; k_3, \omega) \equiv \frac{[U(y_d) - U(y_2)]}{c^2(y_d)} \left(1 - \frac{|y_2 - y_d|}{y_d} b_0\right) + \frac{[\omega^2/U^2(y_2) + k_3^2]}{\sqrt{\omega^2/U^2(y_2) + k_3^2 - k_{\infty}^2}} \frac{i\pi U^2(y_2) b_0}{c_{\infty}^2 U'' y_d} \quad (22)$$

b_0 is a constant relating the even and odd symmetry components of the Fourier transform of $\tilde{\omega}_c$ (see GAL) and $U''(y_d)$ is the second derivative of the mean velocity profile at y_d . We also use this formula for the calculations in this paper.

2.5 Scattered Solution

The scattered solution, $g^{(s)}(\mathbf{y}, \tau | \mathbf{x}, t)$ in the split formula (15), on the other hand, represents the contribution due to presence of the trailing edge and will satisfy streamwise inhomogeneous boundary and jump conditions on the streamwise-discontinuous surface present in the flow.

Imposing appropriate boundary/jump conditions on the plate surface and its downstream extension leads to a Wiener-Hopf problem (eqs. 6.6-6.8 in GAL) for the (temporal, streamwise and spanwise) Fourier transform of $g^{(s)}(\mathbf{y}, \tau | \mathbf{x}, t)$. The general solution to this problem was derived by GAL, but since experiments show that the interaction of a turbulent jet and a trailing edge generates noise at relatively low frequencies, the analysis and computations were simplified by considering the low-frequency limit ($k_1, k_3 = O(k_\infty)$ and $k_\infty \ll O(1)$ for $y_2 = O(1)$). This low-frequency approximation is also adopted in this paper.

2.6 Acoustic Spectrum Formula for Jet-Surface Interaction in Planar Flows

For a two-dimensional jet with a planar mean flow, GAL showed that the acoustic spectrum for jet-surface interaction noise is given by the remarkably simple asymptotic result,

$$I_\omega(\mathbf{x}) \equiv \frac{1}{2\pi} \int_{-\infty}^{\infty} e^{i\omega\tau} \overline{p^s(\mathbf{x}, t) p^s(\mathbf{x}, t + \tau)} d\tau \approx \left(\frac{k_\infty}{4\pi|\mathbf{x}|} \right)^2 \int_0^\infty \int_0^\infty D(\theta, \psi, M(y_2)) S(y_2, \tilde{y}_2; k_3^{(s)}, \omega) dy_2 d\tilde{y}_2, \quad (23)$$

in which the integrand can be interpreted as the product of the source function $S(y_2, \tilde{y}_2; k_3^{(s)}, \omega)$ with a nonuniform directivity factor, $D(\theta, \psi, M(y_2))$, that encapsulates all propagation and surface interaction effects, when $k_\infty \ll O(1)$ and $|\mathbf{x}| \rightarrow \infty$. $M(y_2) = U(y_2)/c_\infty$ denotes the local acoustic Mach number at the position y_2 and the spanwise wavenumber $k_3^{(s)} = k_\infty \sin \theta \cos \psi$ is found by applying the method of stationary phase for the inverse Fourier integral in k_3 (see GAL, p. 553). Here, θ is the polar observation angle measured relative to the jet center line and ψ is the azimuthal angle in the cross-stream plane.

The directivity factor, which is given by

$$D(\theta, \psi, M(y_2)) = \frac{[M(y_2)M(\tilde{y}_2)]^{3/2} (\beta - \cos \theta)}{[1 - M(y_2)\cos \theta][1 - M(\tilde{y}_2)\cos \theta] \sqrt{[1 - \beta M(y_2)][1 - \beta M(\tilde{y}_2)]}}, \quad (24)$$

reduces to Goldstein's (Ref. 15, eq. 3.23) result $\sin^2 \frac{\theta}{2} / [1 - M(y_d)\cos \theta]^2$ at the point where the velocity profile is maximum $y_2 = \tilde{y}_2 = y_d$ since $\beta \equiv (1 - \sin^2 \theta \cos^2 \psi)^{1/2}$, is unity at $\psi = \pm \pi$, in the plane perpendicular to the plate. In Figure 2(a) we show that $D(\theta, \psi, Ma)$ peaks at $\theta = 90^\circ$ for subsonic acoustic Mach numbers. The azimuthal variation of $D(\theta, \psi, Ma)$ possesses dipole-like structure for any point $y_2 = \tilde{y}_2$ (see Figure 2(b)).

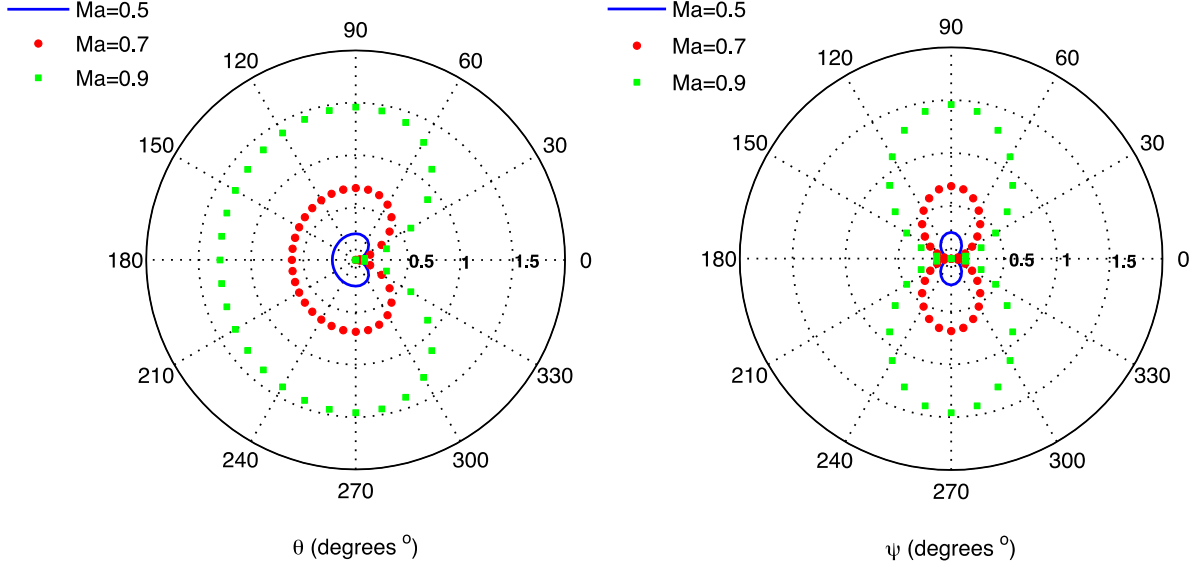


Figure 2.—Directivity factor: (a) θ -directivity, (b) ψ -directivity.

3.0 Physically Realizable Upstream Turbulence Conditions

3.1 Turbulence Model

The jet-surface interaction noise model (23) was constructed for a two-dimensional jet with planar mean flow. Consistent with this approximation, we suppose that the turbulence is spanwise homogeneous. The space-time average

$$\left\langle v_{\perp}^{\prime(0)}(\mathbf{x}, t) v_{\perp}^{\prime(0)}(x_1, \tilde{x}_2, x_3 + \eta_3, t + \tau) \right\rangle \equiv \lim_{T \rightarrow \infty} \frac{1}{2T} \int_{-T}^T \int_{-\infty}^{\infty} v_{\perp}^{\prime(0)}(\mathbf{x}, t) v_{\perp}^{\prime(0)}(x_1, \tilde{x}_2, x_3 + \eta_3, t + \tau) dt dx_3, \quad (25)$$

that enters the integrand of (20) is both experimentally determinable and has a well established database (e.g., experiments reported in Ref. 17).

In this section, we construct a model for this function that is physically realizable and use it to derive a formula for the acoustic spectrum of the trailing edge noise. Different from GAL, however, the present model includes a finite decorrelation region, which we show has a direct impact on the jet surface interaction noise and, in principle, could provide a means to reduce it.

We use the function (Ref. 13):

$$\left\langle \rho v_{\perp}^{\prime(0)}(x_1, y_d, x_3, t) \rho v_{\perp}^{\prime(0)}(\tilde{x}_1, y_d, x_3 + \eta_3, t + \tau) \right\rangle = L_3 \Psi(\bar{x}_1) \left[a_0 + a_1 \tau \frac{\partial}{\partial \tau} + a_2 \eta_1 \frac{\partial}{\partial \eta_1} + \dots \right] e^{-X(\tau, \eta_1, \eta_3)}, \quad (26)$$

where the decay function is,

$$X(\eta_1, \eta_3, \tau) = \sqrt{(\eta_1/l_1)^2 + (\eta_1 - U_c \tau)^2/l_0^2 + (\eta_3/l_3)^2} \quad (27)$$

and the streamwise and spanwise separations are $\eta_1 \equiv \tilde{x}_1 - x_1$ and η_3 , respectively. l_1 and l_3 are turbulence length scales in streamwise and spanwise directions, respectively; l_0 , on the other hand, measures the scale of turbulence as it convects over separation distance η_1 with convection velocity, U_c .

Following GAL we allow Ψ to decay in the streamwise direction in order to insure convergence of the subsequent Fourier transform integrals, i.e., $\Psi(\bar{x}_1) = \Psi_0 e^{-\alpha(\bar{x}_1/L_1)^2}$ where α is a small positive number, $0 \leq \alpha < 1$ which depends on the symmetric location $\bar{x}_1 \equiv (x_1 + \tilde{x}_1)/2$, since we this quantity is expected to be independent of the streamwise coordinate for the nearly parallel flow being considered. Ψ_0 is expected to scale with the transverse component of the mean square turbulence momentum flux $(\overline{\rho v'_1})^2$, L_1, L_3 are geometric spatial scales: L_3 being a measure of the transverse extent of the turbulence and the L_1 , is taken to be large in order to insure that the correlation (26) is relatively independent of \bar{x}_1 to remain consistent with our representation of the upstream boundary condition described in Section 2.0.

As shown in Figure 3, allowing the coefficient $a_1 > 0$ in Equation (26) gives a negative (decorrelation) region for the auto-correlation ($\tau = \eta_3 = 0$) function of (26) which did not appear in the model used in GAL (Eq. 6.46). As mentioned in the Introduction, the presence of this negative region is an expected characteristic of the second-order transverse velocity correlations.

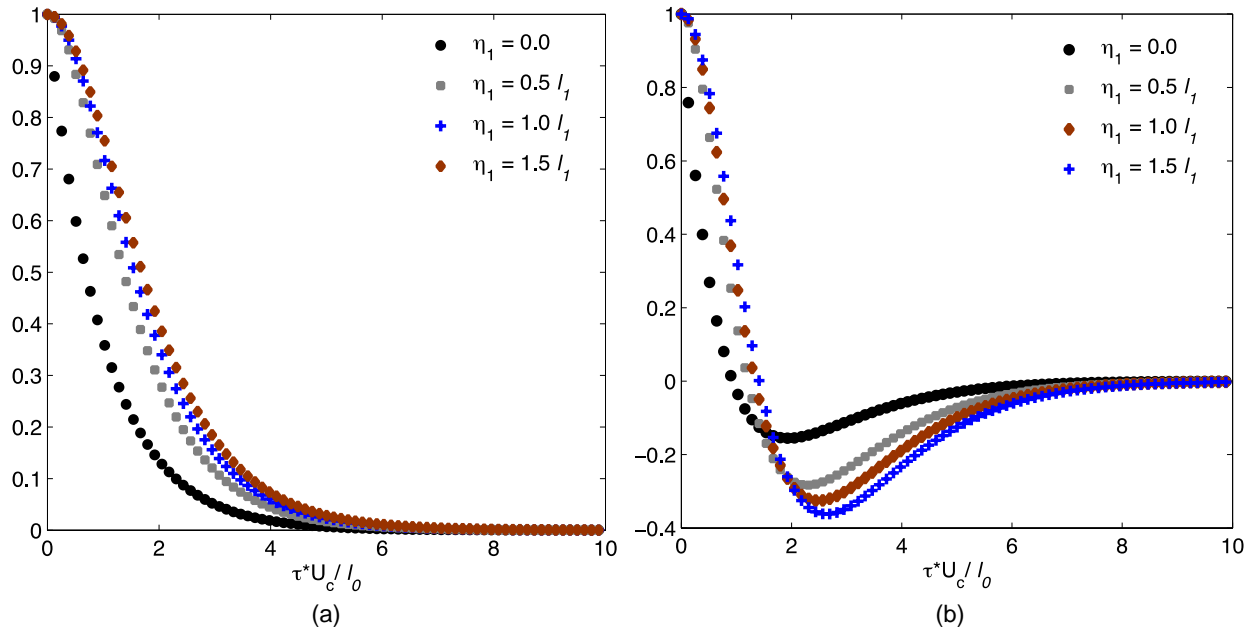


Figure 3.—Turbulence model (26) with (27) for $\tau = \eta_3 = 0$. (a) GAL model $a_1 = a_2 = 0$; (b) Present model $a_1 > 0$.

3.2 Acoustic Spectrum Formula With a Finite Decorrelation Region

Substituting the source model function (23) in (18)-(20) for $S(y_2, \tilde{y}_2; k_3^{(s)}, \omega)$ and inserting this result in (23), we obtain the final formula for the acoustic spectrum used in this paper

$$I_\omega(\mathbf{x}) = \left(\frac{1}{4\pi|\mathbf{x}|} \right)^2 \left(\frac{1}{\pi^2} \right) \frac{l_0 l_1 l_3}{U_c} \left(\frac{L_3 \Psi_0 k_\infty}{c_\infty} \right) (\beta - \cos\theta) I_0(Ma, \theta, \psi) \quad (28)$$

where β is defined below (24) and

$$I_0(Ma, \theta, \psi) = 4 \int_0^{Ma} \frac{c_\infty M(y_2)^3}{[1 - M(y_2) \cos\theta]^2} \frac{\tilde{\Pi}(\omega/U(y_2), \omega, k_3^{(s)})}{|E(y_2; k_3^{(s)}, \omega)|^2 [1 - \beta M(y_2)]} dM(y_2) \quad (29)$$

where $Ma \equiv U(y_d)/c_\infty$ denotes the maximum acoustic Mach number and spectral functions $E(y_2; k_3^{(s)}, \omega)$ is given by (22) and $\tilde{\Pi}(\omega/U(y_2), \omega, k_3^{(s)})$ is defined by:

$$\tilde{\Pi}(k_1, \omega, k_3) = \frac{1}{((\omega l_0/U_c)^2 + \chi)^2} \left[(a_0 - a_1 - a_2) + \frac{4}{((\omega l_0/U_c)^2 + \chi)} \left[a_1 \left(\frac{\omega l_0}{U_c} \right)^2 - \left(a_2 k_1 + a_1 \frac{\omega}{U_c} \right) (k_1 - \omega/U_c) l_1^2 \right] \right] \quad (30)$$

where

$$\chi = \chi(k_1, k_3) = \left[(k_3 l_3)^2 + (k_1 - \omega/U_c)^2 l_1^2 + 1 \right]. \quad (31)$$

The derivation of this formula is summarized in appendix A of Afsar et al. (Ref. 18).

4.0 Low-Frequency Roll-Off

The predictions in GAL were compared against the jet-surface interaction experiments performed at NASA Glenn (Refs. 6, 7, 8, 9, and 10). The relevant geometric parameters are shown in Figure 4.

However it is clear from figure 6 in GAL, that for Strouhal numbers less than 0.15 (where the peak noise amplification occurs), the positive auto-correlation model (i.e., $a_1 = a_2 = 0$ in (26)) they used over predicts the the low frequency roll-off for jet-surface interaction noise by as much as 10 dB (see figure 6d in GAL).

We can easily prove why this occurs by estimating integral $I_0(Ma, \theta, \psi)$ defined by (29), for very small frequencies. As $\omega \rightarrow 0$, the dominant contribution to integral comes in the vicinity of critical level $y_2 = O(y_d)$. In the appendix, we estimate terms in (29) under this limit by considering $\psi = \pm 90^\circ$ (which is the azimuthal location of the data for which the GAL predictions were made); $\beta = 1$ and $k_3^{(s)} = 0$ here. Substituting equation asymptotic properties (38) into acoustic spectrum formula (28) shows that the latter possesses asymptotic properties,

$$I_{\omega}(\mathbf{x}) = \begin{cases} O(1), & \text{for } a_1 = a_2 = 0 \\ O(\omega^2), & \text{for } a_0 \sim a_1 \end{cases} \quad (32)$$

when $\omega \rightarrow 0$ that is now directly dependent on the whether a decorrelation region in (26) exists or not.

In the absence of a decorrelation region in (26) (i.e., $a_1 = a_2 = 0$) the acoustic spectrum does not possess a low frequency roll-off as such and tends to $O(1)$ (i.e., a constant, see equation (6.52) in GAL). A finite decorrelation region, however, increases the low frequency ‘roll-off’ in the prediction of (28) to exhibit an asymptotic order of $O(\omega^2)$ or so, which is more dipole-like and appears to be more consistent with the experimental data. This is shown below in Figure 5 by comparing against experimental data measured at the shielded location with microphone array below plate (Ref. 9) and for a mean velocity profile (Eq. 6.55) used in GAL.

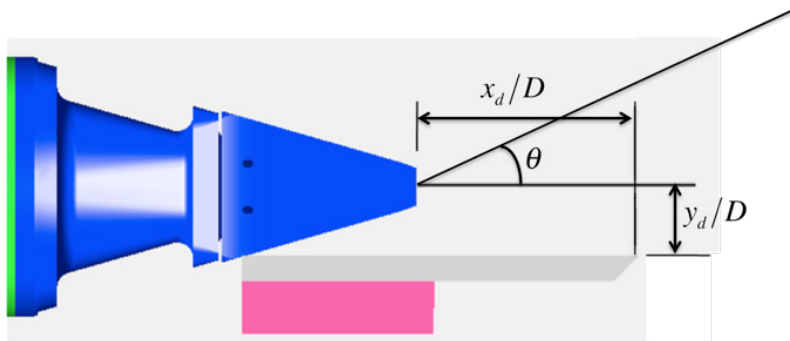


Figure 4.—Nozzle/plate configuration. Figure courtesy Dr. James E. Bridges, NASA Glenn.

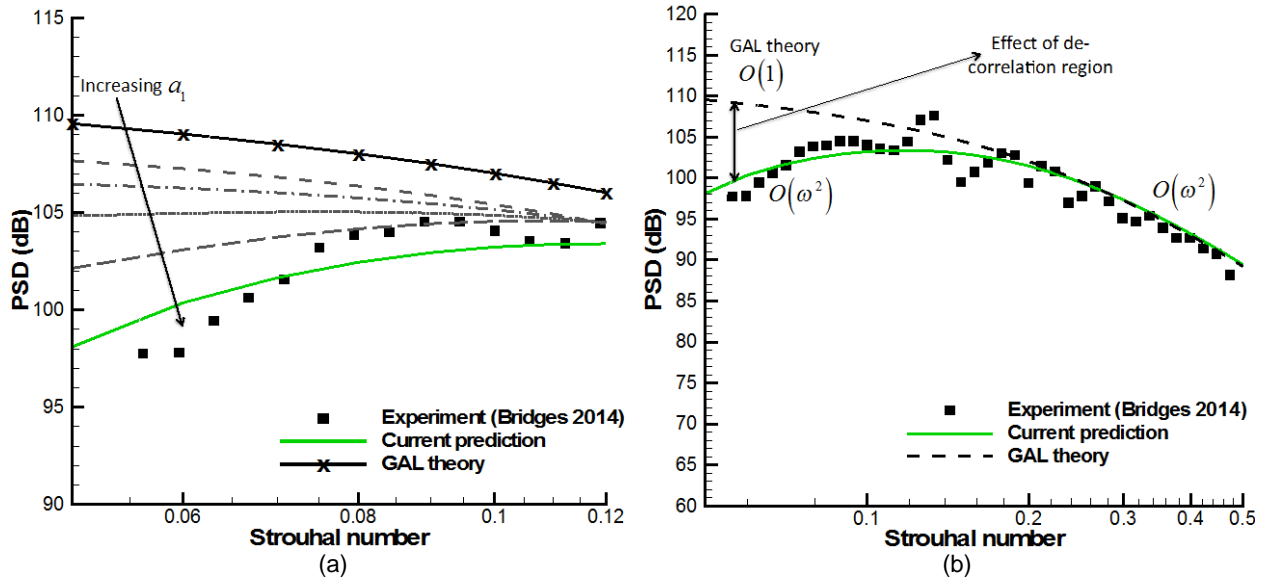


Figure 5.—Power Spectral Density (PSD) of the far-field pressure fluctuations at 100 equivalent diameters from nozzle exit (lossless in dB scale referenced to $20 \mu\text{Pa}$) as a function of Strouhal number, for $Ma = 0.9$. Plate trailing edge at $y_d/D_J = 1.2$, $x_d/D_J = 5.7$, $D_J = 2.12''$, $\psi \pm 90^\circ$ and $\theta = 90^\circ$. Source model constants for GAL theory are the same as their figure 4. Source model constants for current predictions are $\Psi = 0.04(\rho_\infty U_d)^2$; $(l_0, l_1, l_3)/D_J = (0.53, 0.01, 0.01)$; $(L_2, L_3)/D_J = (0.5, 20)$, $U_c = 0.68 U_d$, $b_0 = 0.52$ and $(a_0, a_1, a_2) = (0.82, 0.88, 0.05)$. (a). Parametric increase in a_1 with $a_0 = 1$; $a_2 = 0$. (b). Equation (28) using model (26).

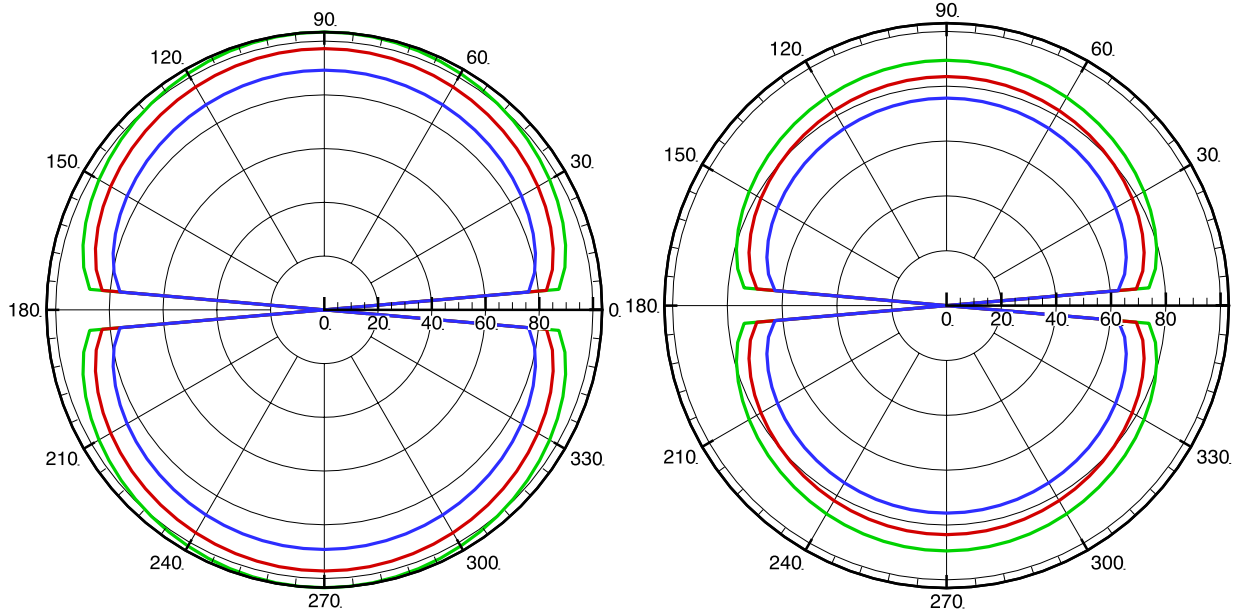


Figure 6.— ψ -directivity of RDT prediction (28) at peak Strouhal number (St) and upper limit as shown in Figure 5 for $M(y_2) = Ma = (0.5, 0.7, 0.9)$ (colour coding same as Figure 2). Source model constants for RDT prediction is same as Figure 5.

In Figure 6 we show that the acoustic spectrum (28) possesses a dipole-like azimuthal structure. Here we consider the polar angle of 90° where the jet-surface interaction noise is greatest and a peak Strouhal number which looking at Figure 5 occurs at about $St=0.12$. The turbulence, defined through the source term $S(y_2, \tilde{y}_2; k_3^{(s)}, \omega)$, amplifies the pure propagation effects described through the directivity factor shown in Figure 2.

Figure 7 shows that even though the GAL theory is based on a two-dimensional mean flow (i.e., on a large aspect ratio rectangular jet nozzle) it provides a reasonable estimate to the lower aspect ratio (AR) jet-surface interaction noise.

5.0 RANS Solutions

Although the RDT predictions based on an analytical mean flow shown in Figure 7 are in reasonable agreement with data, it is expected that the turbulence length scales and peak turbulent kinetic energy levels near the trailing edge will change with nozzle aspect ratio and flow conditions. These variations can be accommodated within the RDT model using a RANS-based mean flow, turbulent kinetic energy (k) and rate of energy dissipation (ϵ) to define the mean velocity profile, length scales and amplitude of the source function, S , near the trailing edge.

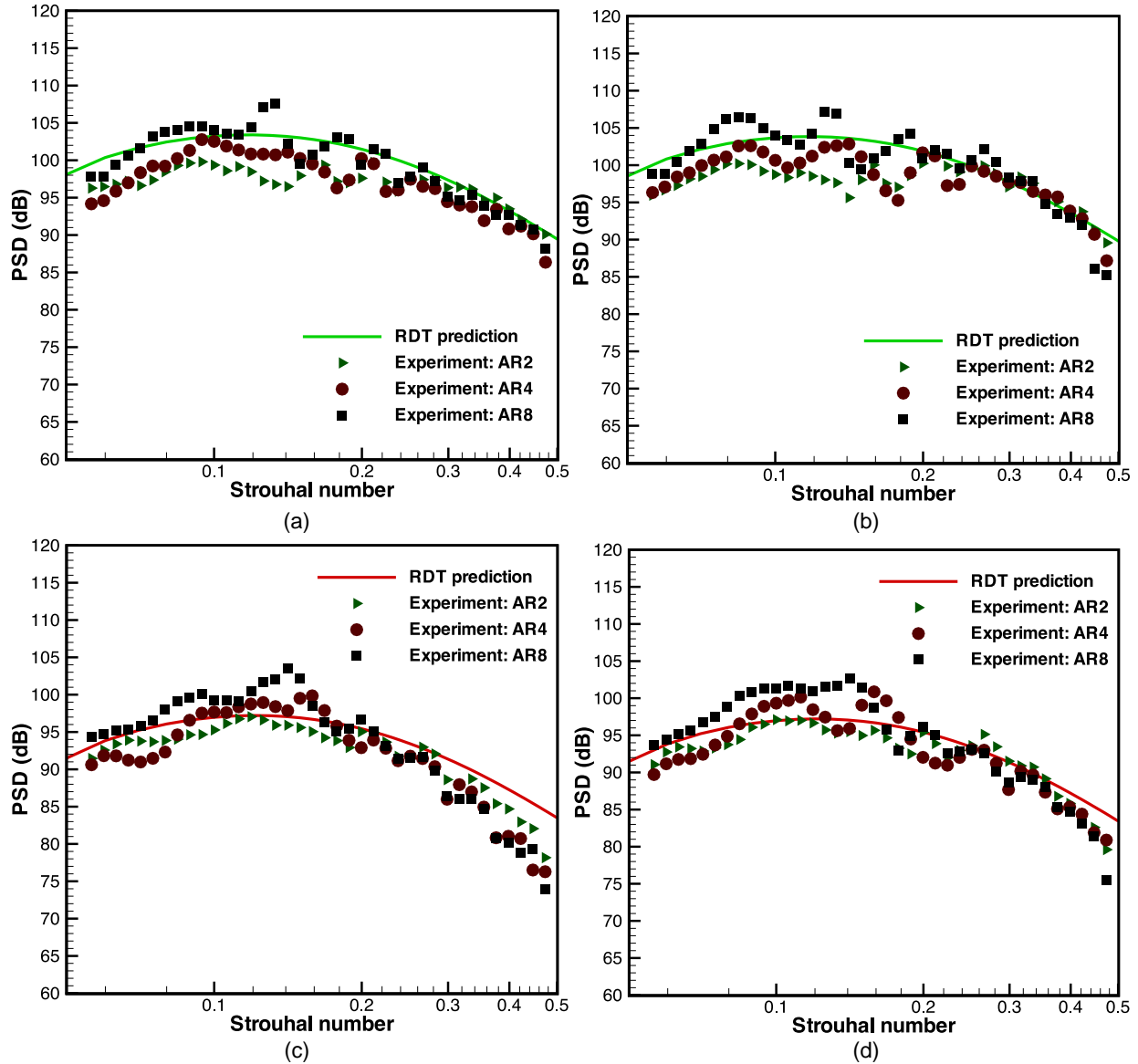


Figure 7.—RDT predictions compared to noise data from various nozzle aspect ratio (AR) rectangular jets. Source model constants and mean flow for RDT prediction is same as Figure 5. (a) $Ma = 0.9$ and $\theta = 90^\circ$. (b) $Ma = 0.9$ and $\theta = 75^\circ$. (c) $Ma = 0.7$ and $\theta = 90^\circ$. (d) $Ma = 0.7$ and $\theta = 75^\circ$.

In this section we show results from three-dimensional SolidWorks Flow Simulations of jet flows with acoustic Mach numbers, $Ma = (0.5, 0.7, 0.9)$ through rectangular jet nozzles with aspect ratios, $AR = (2, 4, 8)$. The SolidWorks Flow Simulation automatic gridding methodology (Refs. 11 and 12) provides a way to mesh and solve the flow field around complex geometries and is, therefore, rather convenient for the jet surface interaction problem. In Figure 8, mean axial velocity and turbulent kinetic energy RANS results are compared with hotwire data from Zaman et al. (Ref. 7). The results are compared for the same aspect ratio (8) and surface length (12-in.), but, owing to facility constraints, at different flow conditions and very slightly different surface offsets. The RANS results have a surface offset of $y_2/D_J = 1.05$, whereas the offset in the experiment is $y_2/D_J = 1.0$. In comparing the RANS and hot-wire data, we have normalized the mean axial velocity and turbulent kinetic energy using the ideally-expanded jet exit velocity as, U_J

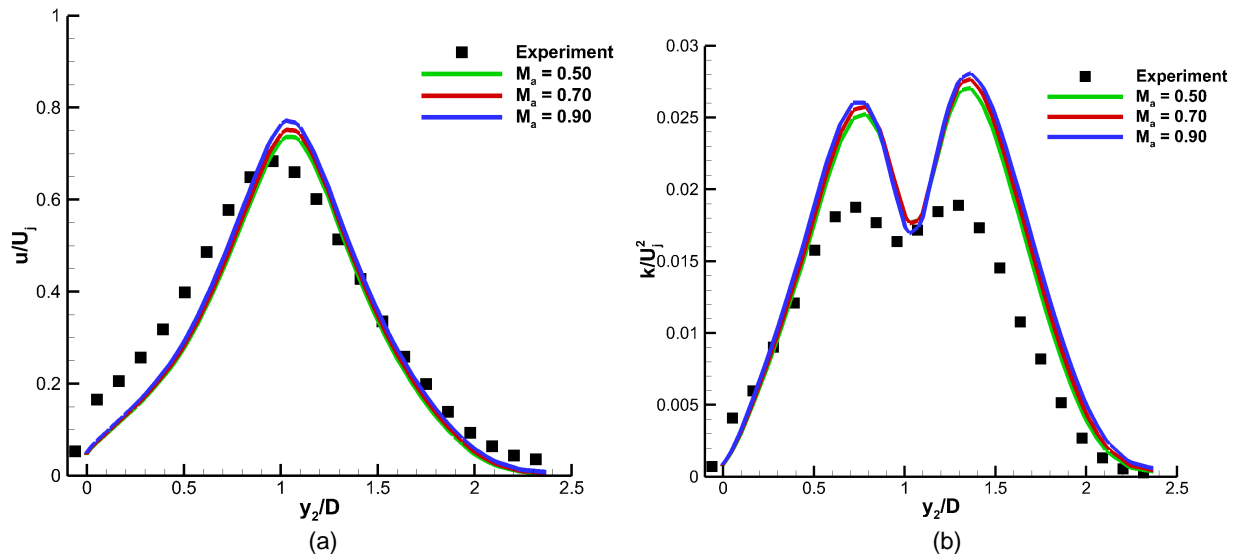


Figure 8.—Comparison of normalized mean flow and turbulent kinetic energy obtained by RANS SolidWorks calculation at the trailing edge location, $y_d/D_J = 1.2$, $x_d/D_J = 5.7$, $D_J = 2.12''$, with low Mach number and high aspect ratio experiment reported in Zaman et al. (Ref. 7), where jet Mach number is $Ma = 0.22$ and $AR = 8$. (a) Mean velocity, U/U_J . (b) Turbulent Kinetic Energy, k/U_J^2 .

and U_J^2 , respectively. It is expected that these normalized results can be reasonably compared to give some idea of the validity of the SolidWorks RANS solutions. Further comparisons are planned once more data becomes available.

The results in Figure 8 show that, while the shapes of the axial velocity and turbulent kinetic energy distributions are well predicted, the peak turbulent kinetic energy is over-predicted by about 35 percent compared to PIV data at the trailing edge location. Nonetheless, these differences are consistent with other RANS CFD codes, such as the NASA WIND code (Ref. 20). Cross flow distributions of mean axial velocity and turbulent kinetic energy, shown in Figure 9, near the surface trailing edge ($x_d/D_J = 5.7$ in Figure 4), compare favorably with the experimental results.

Figure 10 shows values of the normalized RANS-based turbulent kinetic energy and length scale, $L_{RANS} = k^{3/2}/\varepsilon$, at the trailing edge of the plate at the peak mean axial velocity location at the center of the span for $Ma = 0.5, 0.7, 0.9$ and AR_2, AR_4, AR_8 . The results show that the RANS-based turbulent kinetic energy and length scale reduce as the nozzle AR reduces for any given acoustic Mach number. On the other hand, the variation of these normalized scales is relatively insignificant at a fixed nozzle AR and varying acoustic Mach number.

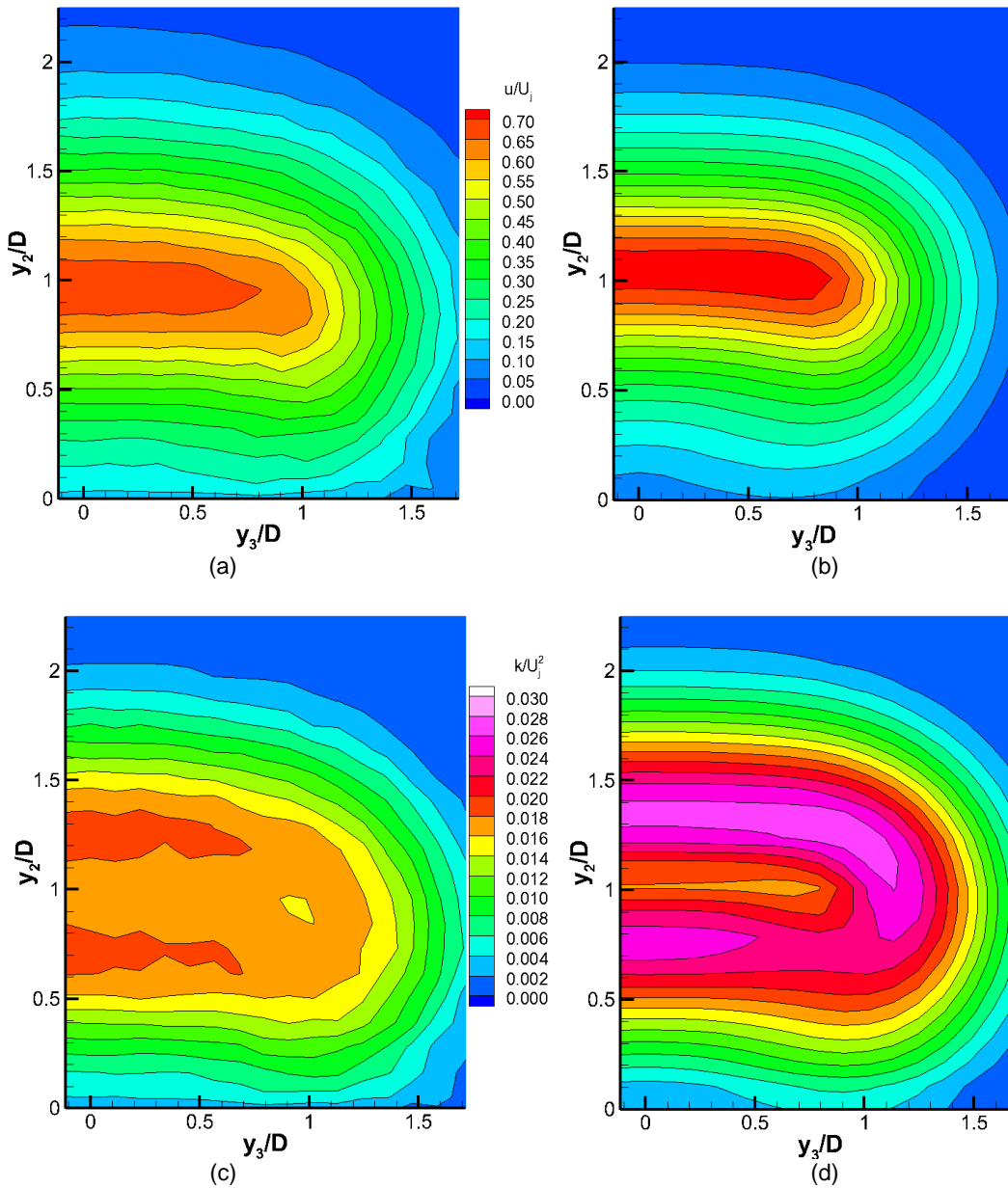


Figure 9.—Comparison of Normalized mean velocity and turbulent kinetic energy obtained by RANS SolidWorks calculation and experiments reported in Zaman et al. (Ref. 7) for same trailing edge location as the caption in Figure 8. (a) U/U_j : Zaman et al. (Ref. 7). (b) U/U_j : RANS calculation. (c) k/U_j^2 : Zaman et al. (Ref. 7). (d) k/U_j^2 : RANS calculation.

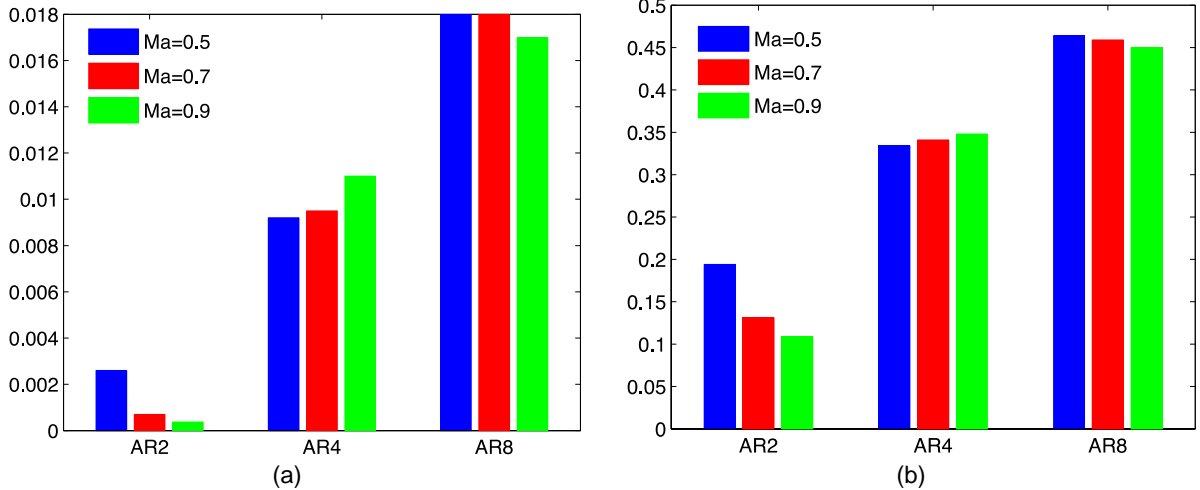


Figure 10.—Variation of normalized turbulent kinetic energy and length scale obtained by RANS SolidWorks calculation with Nozzle Aspect Ratio (AR) and Acoustic Mach number. (a) k/U_j^2 . (b) L_{RANS}/D_J .

6.0 RANS-Based Jet-Surface Interaction Noise Predictions

Using the RANS solutions described in the last section, we define the length scales to be

$$l_n = c_n k^{3/2} / \epsilon, \quad n = 0, 1 \text{ and } 3 \text{ and the amplitude } \Psi_0 = c_\Psi \bar{\rho} k \text{ in the jet-surface interaction model, (28).}$$

Moreover, the mean flow U/U_J is obtained directly from the RANS calculation at the trailing edge of the plate. The scaling coefficients are then tuned so that the predictions at polar angle, $\theta = 90$ and $Ma = 0.9$ (where jet-surface interaction is greatest, see Figure 5 and Figure 7) and $AR8$ for which the theory is directly applicable.

In Figure 11 and Figure 12 we show the RANS-based $\theta = 90$ spectra for $Ma = 0.7$ and $Ma = 0.9$, respectively for aspect ratios $AR4$ and $AR8$. The low frequency roll-off is predicted well for almost all cases shown in Figure 11 and Figure 12. There is a some underprediction of $Ma = 0.7$ and $AR = 4$. They are, however, encouraging given that the model parameters in (28) have been kept fixed at $(c_0, c_1, c_3) = 1.4, 0.021, 0.022$, $U_c = 0.60U_d$, $b_0 = 0.6$, $c_\Psi = 1.0$ and $(a_0, a_1, a_2) = 0.82, 0.88, 0.05$ in all cases, with exception of the spanwise length L_3/D_J , where $L_3/D_J = 10$ for $AR = 4$ case and $L_3/D_J = 20$ for $AR = 8$. The latter reflects the larger spanwise extent of the turbulence in the larger aspect ratio case.

It is expected that, with further experimentation with c_0, c_1, c_3 and c_Ψ , the predictions could, potentially, be made to agree better with the data, especially if the model parameters in (28) are also tuned for each nozzle aspect ratio.

We note that the model does not predict the oscillations that are present in the data at very low frequency. These oscillations are believed to be due to interference between direct and edge-generated sound. In our case, the purely convected disturbance in a streamwise uniform flow (the gust) does not produce direct acoustic radiation at subsonic speeds. However, direct acoustic radiation is produced by the nonpurely convected flow disturbances, i.e., the ‘jet noise.’ This noise is also scattered by the edge and its subsequent interference with the edge-generated noise is most likely responsible for the oscillations seen in the data.

The basic assumption of RDT is that the decay time of the turbulent eddies is short compared to their nonlinear interaction time, which means that the latter unsteadiness (which produces what we refer to as the ‘jet noise’) is being neglected. However, the purely convected gust, which is taken as the input disturbance to the RDT (see Eq. (17)), is much larger than the nonlinear sources of jet noise during the

time over which the interactions take place. As we have shown in this paper, the RDT model predicts the main asymptotic behavior of edge-generated noise and also provides predictions that are within experimental uncertainty over a range of nozzle aspect ratios.

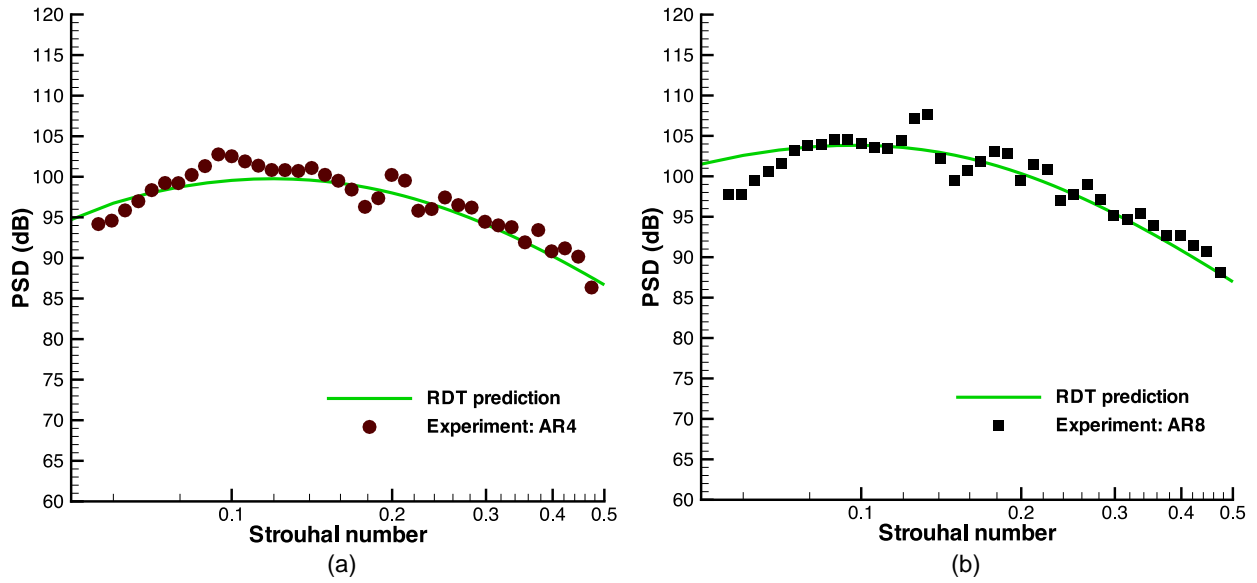


Figure 11.— $\theta = 90^\circ$ spectrum: RDT prediction for $Ma = 0.9$ compared to noise data. (a) $AR = 4$. (b) $AR = 8$.

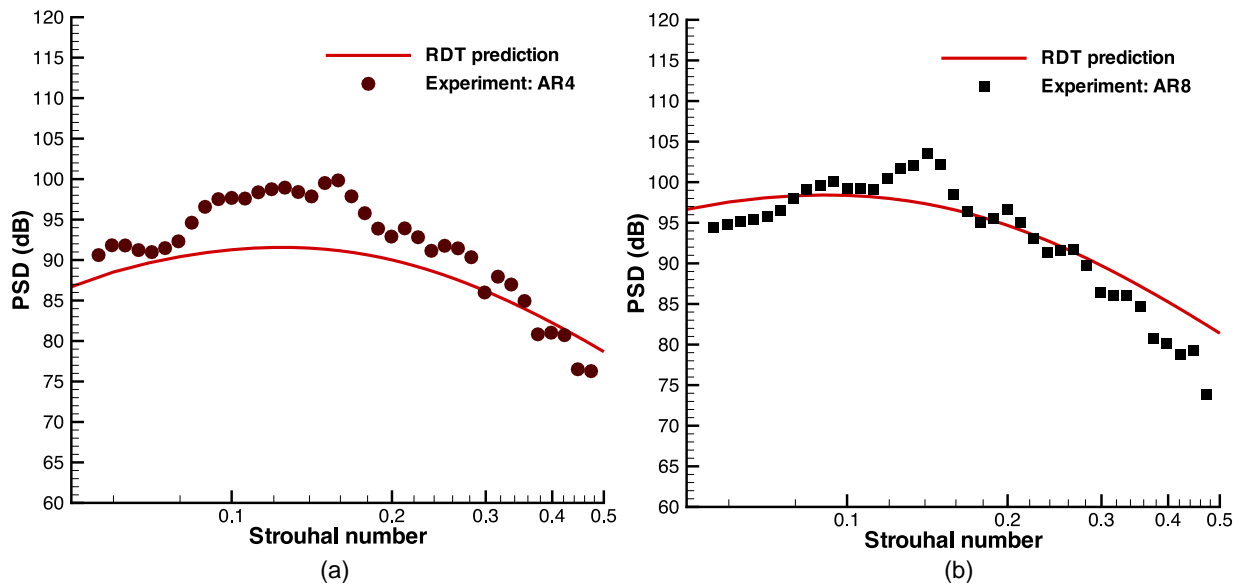


Figure 12.— $\theta = 90^\circ$ spectrum: RDT prediction for $Ma = 0.7$ compared to noise data. (a) $AR = 4$. (b) $AR = 8$.

7.0 Conclusions and Future Work

In this paper we have extended the jet-surface interaction model developed in Reference 1, where it was shown that the jet-surface interaction noise spectrum, $I_\omega(\mathbf{x})$, (28), at the observation point \mathbf{x} , is given by the integral of a directivity factor (24) and a source function, $S(y_2, \tilde{y}_2; k_3^{(s)}, \omega)$, that is related to the upstream turbulence correlation, (25), by the algebraic correspondence relation (21). In this paper we have extended the GAL model to include a finite decorrelation region in the upstream turbulence correlation function (25) by introducing the turbulence model (26) which exhibits properties of type shown in Figure 3 (the auto-correlation of (25)). We have shown, using simple asymptotic arguments and numerical analysis, that the presence of a decorrelation region (i.e., taking $a_1 > 0$ in (26)) directly affects the low-frequency algebraic decay of the jet-surface interaction noise spectrum. This decay, often termed the low frequency ‘roll-off’, must be $O(\omega^2)$ for the acoustic field to be consistent with the dipole-like measured ‘roll-off’ in the experiments reported in Bridges (Ref. 9). A finite decorrelation is required *in our theory* for the roll-off to be $O(\omega^2)$ at very low frequencies where the maximum sound amplification occurs. In contrast, the GAL model (eq. 6.50 in that paper) did not include the decorrelation effect and thereby produced a spectrum that tends to $O(1)$ at very low frequencies, which is at worst 10 dB greater than experiment (see Figure 5(b)).

The model we have used in this paper, (29), also gives predictions that are reasonably accurate for more three-dimensional flows associated with lower aspect ratio rectangular jets (Figure 7). In addition we have implemented a RANS-based RDT prediction method that takes into account the reduction in length scales and turbulent kinetic energy with nozzle aspect ratio predicted by these flow solutions. This approach generally gives predictions within experimental uncertainty. In principle, any empiricism introduced by tuning the scales from RANS calculation could be eliminated by using experimental or LES data on turbulence (as, for example in Ref. 19).

Professor J.T. Stuart¹ recently pointed out that the importance of any noise prediction model is in its ability to show how to reduce the far-field noise. The jet-surface interaction model (28) based on the nonhomogeneous rapid-distortion theory (RDT) allows the “exact” turbulence conditions to be specified as its upstream boundary condition through the algebraic relation (21) that is a function of the two-point time-delayed correlation (25) of the stationary random function $\rho v'_\perp(\mathbf{x}, t)$ (transverse momentum fluctuation), which Tennekes and Lumley (Ref. 14) explained must go negative with increase in spatial separation and/or time delay in a time-stationary turbulence field. The parametric study in figure 4.1a shows that varying the decorrelation region (increasing coefficient, a_1) varies the predictions so that they lie between GAL model ($a_1 = 0$) to the present results (figure 4.1b) which possesses the correct $O(\omega^2)$ low frequency roll-off. In principle, however, further increases in a_1 , could provide a means to reduce the low frequency amplification associated with jet-surface interaction.

¹ Private communication.

Appendix

Equation (22) shows that $E(y_2; k_3^{(s)}, \omega)$ expands as

$$E(y_2; 0, \omega) \equiv \frac{1}{c_\infty^2} ([U(y_d) - U(y_2)] + i\omega S) + O(y_2 - y_d) \quad (33)$$

since $U(y_2) = U(y_d) + O(y_2 - y_d)$ and $c^2(y_2) = c_\infty^2 + O(y_2 - y_d)$ when $y_2 = O(y_d)$, where $S(y_d)$ is given by

$$S(y_d) = \frac{\pi c_\infty U_d b_0}{U'' y_d \sqrt{c_\infty^2 - U_d^2}} \quad (34)$$

Integral (29) then expands as

$$I_0(Ma, \theta, \pm\pi/2) = 4 \frac{c_\infty Ma^3 \tilde{\Pi}(\omega/U_d, \omega, 0)}{(1 - Ma \cos \theta)^2 (1 - Ma)} \int_0^{Ma} \frac{1}{|E(y_2; 0, \omega)|^2} dM(y_2), \quad \text{for } y_2 = O(y_d) \quad (35)$$

where $Ma = M(y_d)$ and $U_d = U(y_d)$. Inserting (33) result into this latter integral shows:

$$\begin{aligned} I_0(Ma, \theta, \pm\pi/2) &\approx \\ &4 \frac{c_\infty U_d^3 \tilde{\Pi}(\omega/U_d, \omega, 0)}{(1 - Ma \cos \theta)^2 (1 - Ma)} \int_0^{U_d} \frac{1}{[U(y_d) - U(y_2)]^2 + (\omega S)^2} dU(y_2), \\ &= 4 \frac{c_\infty U_d^3 \tilde{\Pi}(\omega/U_d, \omega, 0)}{(1 - Ma \cos \theta)^2 (1 - Ma)} \frac{\pi}{2\omega S}, \quad \text{for } y_2 = O(y_d) \end{aligned} \quad (36)$$

The integral in (36) is now $O(1/\omega)$ where $S = O(1)$. Given that Equation (31) shows $\chi(\omega/U_d, 0) \rightarrow 1$ as $\omega \rightarrow 0$, the function, $\tilde{\Pi}(\omega/U_d, \omega, 0)$ (using (30)) expands as,

$$\tilde{\Pi}(\omega/U_d, \omega, 0) \sim \begin{cases} 1, & \text{for } a_1 = a_2 = 0 \\ \omega^2, & \text{for } a_0 \sim a_1 \end{cases} \quad (37)$$

and, therefore, integral (29) possesses asymptotic properties:

$$I_0(Ma, \theta, \pm\pi/2) \sim \begin{cases} 1/\omega, & \text{for } a_1 = a_2 = 0 \\ \omega, & \text{for } a_0 \sim a_1 \end{cases} \quad (38)$$

when $\omega \rightarrow 0$.

References

1. Goldstein, M. E., Afsar, M. Z. and Leib, S. J., “Non-Homogeneous Rapid Distortion Theory on Transversely Sheared Mean Flows,” *Journal of Fluid Mechanics*, vol. 736, 2013, pp. 532-569.
2. Olsen, W. and Boldman, D., “Trailing edge noise data with comparison to theory,” AIAA Paper 79-1524, 1979.
3. Wang, M.E., “Wing effect on jet noise propagation,” *J. Aircraft*, Vol. 18, No. 4, pp. 295 – 302, 1981.
4. Ffowcs Williams, J. E. and Hall, L. H., “Aerodynamic Sound Generation by Turbulent Flow in the Vicinity of a Scattering Half Plane,” *Journal of Fluid Mechanics*, Vol. 40, pp. 657-670, 1970.
5. Brown, C., ‘Jet-surface interaction test: far-field noise results,’ GT2012-69639: ASME IGTI Turbo Expo, June 11-15, 2012
6. Bridges, J.E., Brown, C. A. and Bozak, R., “Experiments on Exhaust Noise of Tightly Integrated Propulsion Systems,” AIAA Paper 2014-2904, 2014.
7. Zaman, K. B. M. Q., Brown, C. A.; Bridges, J. E., “Interaction of a Rectangular Jet with a Flat-plate Placed Parallel to the Flow,” AIAA Paper 2013-2184, 2013.
8. Zaman, K. B. M. Q., Fagan, A., Clem, M and Brown, C. A., “Resonant Interaction of a Rectangular Jet with a Flat-plate,” AIAA Paper 2014-0877, 2014.
9. Bridges, J., “Noise from Aft Deck Exhaust Nozzles – Differences in Experimental Embodiments,” AIAA Paper 2014-0876, 2014.
10. Brown, C., “Developing an Empirical Model for Jet-Surface Interaction Noise,” AIAA paper 2014-0878, 2014.
11. “Advanced Boundary Cartesian Meshing Technology in SolidWorks Flow Simulation” Dassault Systemes SolidWorks Corporation Technical Paper.
12. “Enhanced Turbulence Modelling in SolidWorks Flow Simulation” Dassault Systemes SolidWorks Corporation Technical Paper.
13. Leib, S.J. and Goldstein, M.E., “Hybrid Source Model for Predicting High-Speed Jet Noise,” *AIAA Journal*, Vol. 49, No. 7, pp. 1324-1335, 2011
14. Tennekes, H. and Lumley, J., *A first course in turbulence*, MIT Press, Cambridge, Mass. 1971.
15. Goldstein, M.E., “Scattering and Distortion of the Unsteady Motion on Transversely Sheared Mean Flows,” *J. Fluid Mech.* Vol. 91, pp. 601-632, 1979.
16. Goldstein, M. E., *Aeroacoustics*, McGraw Hill, New York, 1976.
17. Bridges, J, and Brown, C.A., “Validation of the small Hot jet Rig for Jet Noise Research,” AIAA Paper 2005-2846, 2005.
18. Afsar, M.Z., Leib, S. J. and Bozak, R.F., “Low frequency roll-off of the jet-surface interaction noise spectrum in high-speed rectangular air jets,” To be submitted to *J. Sound and Vib.*
19. Karabasov, S.A., Afsar, M.Z., Hynes, T.P., Dowlong, A.P., McMullan, W.A., Pokora, C.D., Page, G.J. and McGuirk, J.J, “Jet Noise: Acoustic Analogy Informed by Large Eddy Simulation,” *AIAA Journal*, Vol. 48, No. 7, pp. 1312-1325, 2010.
20. Dippold, V., “Acoustic Reference Nozzle with Mach 0.97, Unheated Jet Flow,” NPARC Alliance Validation Archive, NASA Glenn Research Center, <http://www.grc.nasa.gov/WWW/wind/valid/arn/index.html>

